JOURNAL OF SOLID STATE CHEMISTRY 106, 443–450 (1993)

Effect of the Preparation Method on the Oxidation–Reduction Mechanism and the Cation Distribution of Mn–Zn Ferrites

B. GILLOT

Laboratoire de Recherche sur la Réactivité des Solides, URA 23 CNRS, Faculté des Sciences Mirande, B.P. 138, 21004 Dijon Cedex, France

AND M. EL GUENDOUZI

Université Hassan II, Faculté des Sciences II, B.P. 6621, Casablanca, Morocco

Received October 14, 1992; accepted February 16, 1993

The cation distribution of manganese–zinc ferrite $Mn_{0.50}Zn_{0.15}Fe_{2.05}O_4$ prepared by a ceramic route and wet method was investigated by derivative thermogravimetry (DTG) and X-ray diffraction analyses. Below about 500°C, these ferrites which are oxidized in cation deficient spinels show an incomplete oxidation of tetrahedral Mn^{2+} ions leading to a cation distribution $(Zn^{2+}_{0.43}Mn^{2+}_{0.15}Fe^{3+}_{0.42})_A$ $(Fe^{3+}_{1.54}Mn^{3+}_{0.32}\square_{0.14})_B O^{2-}_4$. With increasing temperature further oxidation of Mn^{2+} ions results in the appearance of a rhombohedral phase α-$(Fe_{2-z}Mn_z)O_3$ rich in iron accompanied by a spinel phase containing the totality of zinc.

Introduction

Valence states of manganese and iron and their distribution on both octahedral (*B*) and tetrahedral (*A*) sites of the manganese zinc ferrites with spinel structure have been the subject of many studies because of their interesting electromagnetic properties. However, to obtain accurate electromagnetic properties such as high permeability and low losses, the Mn–Zn ferrites microstructure has to be strictly controlled (*1, 2*). It has been recently established that among the numerous factors acting upon microstructure, which is influenced by all steps in the processing route, the control of the rise in temperature is of fundamental importance, i.e., the rise in temperature below 550°C (*3*). Indeed, in this first zone of sintering, these oxides that are subjected to oxidation–reduction reactions depending principally on cationic distribution (*4*) could lead, because the local densification relative to the chemical reactions are inhomogeneous in the core, to elastic deformations, stresses, and cracks which are in direct relation with the availability for oxidation of manganese ions.

The determination of the valence state of the manganese ions in these compounds is therefore of interest. However, depending on the Zn concentration and preparation methods (ceramic route and wet process), controversy surrounds the question of the coexistence of trivalent manganese with the presence of divalent iron as indicated by neutron diffraction (*5*), Mössbauer spectroscopy (*6*), nuclear magnetic resonance (*7*), and X-ray diffraction (*8*).

We have addressed the question of the cation distribution in Mn–Zn ferrites prepared by different routes with different grain

0022-4596/93 $5.00

TABLE I
SAMPLE CHARACTERISTICS

Samples	Global composition	Specific surface area (m^2/g)	Crystallite size (μm)	Lattice parameter of initial phases (nm)	Lattice parameter of oxidized phases at 450°C (nm)
A	$Mn_{0.50}Zn_{0.45}Fe_{2.05}O_4$	4.6	3	0.8478	0.8407
B	$Mn_{0.50}Zn_{0.44}Fe_{2.08}O_4$	8.2	0.7	0.8477	0.8404
C	$Mn_{0.50}Zn_{0.45}Fe_{2.05}O_4$	25	0.05	0.8475	0.8413
D	$Mn_{0.50}Zn_{0.50}Fe_2O_4$	60	0.02	0.8443	0.8401

sizes by performing a quantitative analysis of oxidizable cations using derivative thermogravimetry. This method, which is based on the discrepancy of reactivity toward oxygen of iron and manganese ions in relation to occupied sites, is especially suited to this purpose due to the fact that it is possible to make a systematic study of the oxidation process in regard with the nature, charge, and position of cation in spinel lattice (*4*).

Experimental

Four samples having approximately the same manganese and zinc concentration (Table I) were prepared by different methods:

—in the past (sample A), the Mn–Zn ferrite was prepared by presintering from a mixture of Fe_2O_3, Mn_2O_3, and ZnO following a procedure previously reported (*9*). The presintering was realized under nitrogen at 1200°C for a period of 3 hr and quenched. The powders have been pounded in an attritor to obtain a specific surface area of about 4.6 m^2/g.

—In the second method (sample B), the spinel was also prepared by the conventional ceramic route according to Michalk (*10*) where oxide raw materials $MnCO_3$, ZnO, and Fe_2O_3 were mixed and fired for 2 hr at 800°C in a vacuum of 10^{-5} Pa and then quenched. This method produces Mn–Zn ferrite with grain sizes smaller than 1 μm (Table I).

—In the third method (sample C), the Mn–Zn ferrite was made in continuation of our studies on the low-temperature preparation of substituted magnetites using oxalate precursors (*11*). The thermal decomposition of mixed manganese–zinc iron oxalates leads, through appropriate thermal treatments at low temperature (<500°C), to the spinel with the desired composition. The sample consists of almost spherical grains of average 0.05 μm (Table I).

—For the fourth sample (sample D), we have adopted the thermal decomposition of the hydrazine precursors, $(N_2H_5)_3Mn_xZn_{1-x}Fe_2(N_2H_3COO)_9 \cdot 3H_2O$, where $x = 0.50$, as described by Suresh *et al.* (*12*). The precursors decompose in single step at about 200°C and produce average crystallite size below 0.02 μm.

The XRD analysis performed with an automatic Siemens diffractometer using Cu radiation, allowed us to verify purity and to measure the lattice parameter of the prepared ferrites before and after oxidation at 420°C (Table I). The formed phases during oxidation were also analyzed by X-ray diffraction of samples cooled from various temperatures in the TG apparatus. Electron microprobe analysis was used to determine the composition of the rhombohedral precipitated phase. The oxidation was performed on a microbalance Setaram MTB 10-

8 with 6 mg of powder with a linear rate of 2.5°C min^{-1}.

Results and Discussion

We have previously determined the cationic distribution of Mn—Zn ferrites of formula $Mn_xZn_yFe_{2.05}O_4$ with $0 < x + y < 0.95$ prepared by a standard ceramic route (sample A) in considering that the Zn^{2+}, Mn^{2+} ions are located on A sites and that the Mn^{3+}, Fe^{2+} ions are on B sites when only the Fe^{3+} ions are distributed among both sites. X-ray diffraction analysis and thermogravimetric data indicate a cation distribution according to the formula:

$$(Mn^{2+}_{0.8x}Zn^{2+}_{y}Fe^{3+}_{1-0.8x-y})_A \quad (Fe^{3+}_{1+0.6x+y}Fe^{2+}_{1-0.8x-y}Mn^{3+}_{0.2x})_B O^{2-}_4 . \quad (1)$$

It was demonstrated that Fe^{2+}_B, Mn^{3+}_B, and Mn^{2+}_A are successively oxidized to five distinct oxidation reactions:

$3Fe^{2+} \rightarrow 2Fe^{3+} + \square$ complete at 280°C
$4Mn^{3+} \rightarrow 3Mn^{4+} + \square$ complete at 330°C
$3Mn^{2+} \rightarrow 2Mn^{3+} + \square$ partial at 360°C
$\square + 3Mn^{4+} \rightarrow 4Mn^{3+}$ complete at 420°C
$3Mn^{2+} \rightarrow 2Mn^{3+} + \square$ complete at 600°C.

Figure 1 compares the mass variation, Δm, when the different manganese–zinc ferrites with $x = 0.5$ were heated in air at a constant rate of 2.5 min^{-1}. As already reported for manganese-substituted magnetites (*4*), three regions can be distinguished. In region I the mass gain is due to total oxidation of Fe^{2+} ions and Mn^{3+} ions on B sites and a partial oxidation of Mn^{2+} ions into Mn^{3+} ions on A sites. Above about 430°C (region II) the spinel starts to lose mass which corresponds to the reduction of Mn^{4+} to Mn^{3+} ions. In region III, we again have a mass gain due to the oxidation of Mn^{2+} ions not being completely oxidized in region I. Although the particle size differs appreciably for samples prepared for ceramic method (samples A and B) and samples obtained by wet chemical process (samples C and D), the observed oxidation–reduction phenomena are similar. The major difference referred to crystallite size originates in beginning of oxidation temperature in region I which strongly decreases with temperature preparation. For I and II regions, X-ray diffraction shows a single phase of spinel structure whereas a spinel phase and a phase of corundum structure containing both Fe and Mn together were present in region III.

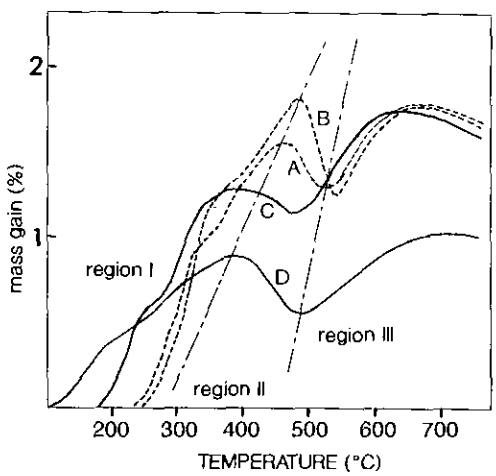

FIG. 1. TG curves for Mn–Zn ferrites prepared by various methods and heated in air at 2.5°C min^{-1}.

In order to estimate the amount of each oxidized cation, a quantitative analysis from the DTG peaks (Figs. 2 and 3) was effected to separate the overlapping weight changes. This was made following the procedure indicated in (*13*) by calculating the S_i/S_0 ratio, where S_i represents the area of each peak and S_0 the area corresponding to pure magnetite ($x = 0$, $y = 0$). The S_i/S_0 ratios are listed in Tables II and III. For samples A, B, and C, it can be seen that the S_i/S_0 ratio of the fourth peak corresponds closely to S_i/S_0 ratio of the second peak. Thus, it is possible to assume that the amount of Mn^{4+} ions created by oxidation of Mn^{3+} ions in region I must be totally reduced to lower valency, i.e. Mn^{3+} ions during the reduction process in region II.

The amount of divalent manganese present in the site A can be calculated by differ-

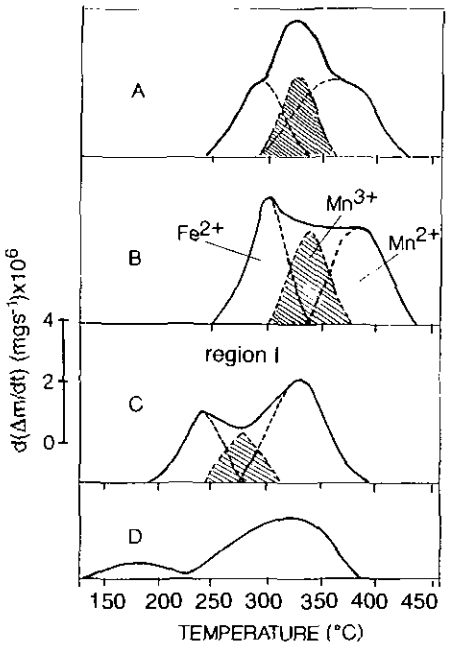

FIG. 2. DTG curves $d(\Delta m/dt) = f(T)$ (—) in region I and desummation spectra (---) of oxidation processes for Fe^{2+} and Mn^{3+} ions on *B* sites and Mn^{2+} ions on *A* sites.

ence with total manganese content. The S_i/S_0 value corresponding to third peak does not agree with the concentration of Mn^{2+} ions and is always lower than that calculated indicating an incomplete oxidation of Mn^{2+} ions in region I. The reoxidized amount in region III was thus explained by comparing the S_i/S_0 ratio of the fifth peak with that of third peak. Total amount of oxidized Mn^{2+} ions is comparable to the concentration of Mn^{2+} ions deduced from global composition. These results for the iron and manganese concentration, assuming that manganese trivalent are preferentially located in *B*-sites, indicate a cation distribution according to the formulae

—Sample A:

$$(Mn^{2+}_{0.40}\, Zn^{2+}_{0.45}\, Fe^{3+}_{0.15})_A \quad (Fe^{3+}_{1.75}\, Fe^{2+}_{0.15}\, Mn^{3+}_{0.10})_B\, O^{2-}_4 . \quad (2)$$

—Sample B:

$$(Mn^{2+}_{0.35}\, Zn^{2+}_{0.44}\, Fe^{3+}_{0.21})_A \quad (Fe^{3+}_{1.64}\, Fe^{2+}_{0.21}\, Mn^{3+}_{0.15})_B\, O^{2-}_4 . \quad (3)$$

—Sample C:

$$(Mn^{2+}_{0.44}\, Zn^{2+}_{0.45}\, Fe^{3+}_{0.11})_A \quad (Fe^{3+}_{1.83}\, Fe^{2+}_{0.11}\, Mn^{3+}_{0.06})_B\, O^{2-}_4 . \quad (4)$$

For sample D prepared at lower temperature it appeared that the area ratio of the first and second peak (Table II) has diminished an appreciable degree suggesting a partial oxidation of Fe^{2+} ions and total oxidation of Mn^{3+} ions whereas the S_i/S_0 ratio of the third peak remains unchanged. This is probably due to a larger specific surface area that induces an oxidation in air at room temperature of cations located in *B* sites (*13*). The formula for sample D is best described by:

$$(Mn^{2+}_{0.39}\, Zn^{2+}_{0.49}\, Fe^{3+}_{0.12})_A \quad (Mn^{4+}_{0.10}\, Fe^{2+}_{0.034}\, Fe^{3+}_{1.807}\, \square_{0.061})_B\, O^{2-}_4 . \quad (5)$$

The lattice parameter was found to be 0.8443 nm and is significantly smaller that the 0.8477 nm value obtained for other samples (Table I) according to the partial oxidation of this sample.

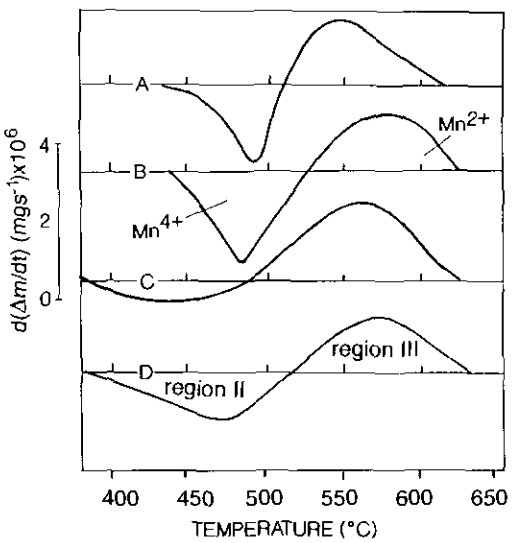

FIG. 3. DTG curves $d(\Delta m/dt) = f(T)$ in regions II and III.

TABLE II

DEPENDENCE OF S_i/S_0 RATIO AND OXIDATION TEMPERATURE OF EACH PEAK IN REGION I FOR VARIOUS METHODS OF PREPARATION

	Region I					
	First peak (Fe^{2+})		Second peak (Mn^{3+})		Third peak (MN^{2+})	
Samples	S_i/S_0	T_{ox} (°C)	S_i/S_0	T_{ox} (°C)	S_i/S_0	T_{ox} (°C)
A	0.15	290	0.10	325	0.24	363
B	0.21	302	0.14	338	0.21	385
C	0.10	243	0.06	278	0.22	330
D	0.03	180	0	—	0.23	300

The experimental evolutions of the lattice parameter recorded at various levels of oxidation (Fig. 4) between 100 and 700°C show that for all samples the lattice parameters strongly decrease in region I which is consistent with the incorporation of vacancies in the spinel lattice. In region II the spinel structure was also maintained but the lattice parameter slightly increases according to a reduction process in this temperature range which decreases the cation vacancy content. At higher temperatures (region III), the lattice parameter increases more rapidly (Fig. 4, curve a) that can be correlated with the curve b which shows the percentage of rhombohedral phase α-$(Fe_{2-z}Mn_z)_2\ O_3$ precipitated and accompanying the spinel phase containing the totality of zinc. It should be emphasized that for this Mn content, a low solubility of Mn_2O_3 in α-Fe_2O_3 has been advanced (*14*) although the presence of Mn does not greatly modify the lattice parameter of α-Fe_2O_3.

These results clearly indicate that the phase change above 530°C is associated with the oxidation of Mn^{2+} ions that were not completely oxidized at a lower temperature. In these conditions and for 60% of Mn^{2+} ions oxidized in region I, the ion distribution for samples oxidized in region II (i.e., samples C) without phase transformation is given by the formula:

$$(Zn^{2+}_{0.429}Mn^{2+}_{0.152}Fe^{3+}_{0.419})_A\ (Fe^{3+}_{1.536}Mn^{3+}_{0.325}\square_{0.139})_B\ O^{2-}_4 \quad (6)$$

with an experimental parameter of 0.8413 nm.

TABLE III

DEPENDENCE OF S_i/S_0 RATIO AND OXIDATION TEMPERATURE OF FOURTH AND FIFTH PEAKS IN REGIONS II AND III

	Region II fourth peak (Mn^{4+})		Region III fifth peak (Mn^{2+})		% Mn^{2+} ions oxidized
Samples	S_i/S_0	T_{ox} (°C)	S_i/S_0	T_{ox}(°C)	in region I
A	10	493	16	545	60
B	15	480	14	579	60
C	0.06	465	22	574	55
D	17	475	16	577	53

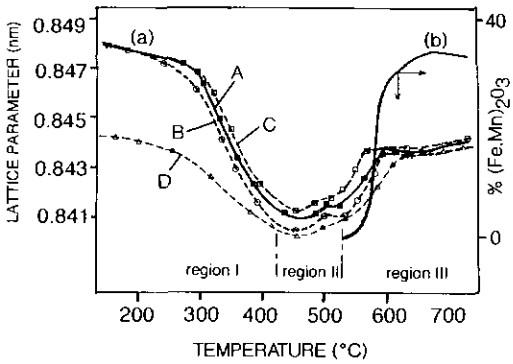

FIG. 4. Evolution of lattice parameters (curve a) as a function of oxidation temperature. The curve b shows the percentage of α-$(Fe_{2-z}Mn_z)O_3$ precipitated in region III for sample A.

It is informative at this stage to compare the results obtained in this work with those reported previously and that for the same Mn content (*15*, *16*). The striking discrepancy concerns the vacancy content which was found to have a significant occupancy in the original study and consequential affect on the phase change. It is argued that the phase change to proceed primarily after total oxidation of all oxidizable cations and results from the cation deficient spinel:

$$(Zn^{2+}_{0.421}Fe^{3+}_{0.579})_A\,(Mn^{3+}_{0.440}Fe^{3+}_{1.373}\square_{0.187})_B\,O^{2-}_4 \qquad (7)$$

leading to the formation of two clusters:

cluster I $(Fe^{3+}_{0.89}\square_{0.11})_A$

$$(Mn^{3+}_{0.440}Fe^{3+}_{1.34}\square_{0.22})_B\,O^{2-}_4 \qquad (8)$$

cluster II $(Zn^{2+}_{0.97}\,Fe^{3+}_{0.03})_A$

$$(Mn^{3+}_{0.440}Fe^{3+}_{1.56})_B\,O^{2-}_4 \qquad (9)$$

with lattice parameters of 0.8383 and 0.8439 nm, respectively.

It is possible to calculate by the Poix method (*17*) the theoretical lattice parameter for the two distributions. This method consists of calculating the crystal lattice parameter from cation–anion bond lengths. The cation–oxygen distance of Mn^{2+}, Fe^{3+}, Zn^{2+}, and vacancy on *A* sites as well as the cation–oxygen distance of Mn^{3+}, Fe^{3+}, and vacancy on *B* sites are listed in Table IV. The theoretical lattice parameters calculated for I and II clusters are given in Table V (columns 5 and 6). For cluster II, one obtains a similar value to that determined in (*15*) but for cluster I, the calculated value appears lower whatever the location of vacancies in the spinel lattice (0.8363 nm for the distribution $\frac{2}{3}\square$ on *B* sites and $\frac{1}{3}\square$ on *A* sites and 0.8360 nm with the totality of vacancies on *B* sites).

Since the presence of vacancies decreases the unit cell [18], we can think that the vacancy concentration is lower than that reported, i.e., 0.14 per "molecule" instead of 0.187. In this respect we can speculate on the phase change in region III and the uncertainties regarding the elimination of vacancies resulting of the simultaneous formation of a spinel and rhombohedral phases during the oxidation of remaining Mn^{2+} ions. Just before the phase transformation, the calculated and theoretical lattice parameters have the same value (Table V, column 3) but slightly differs within the temperature range 550–620°C corresponding to region III.

On the basis of results obtained by electron microprobe analysis at 620°C which give the at.% of different metallic elements, the formula of the rhombohedral precipitated phase may be considered to be:

$$\alpha\text{-}(Fe^{3+}_{1.70}Mn^{3+}_{0.30})\,O_3 \qquad (10)$$

TABLE IV

CATION–OXYGEN DISTANCES USED FOR LATTICE PARAMETER CALCULATIONS

	Cation–oxygen distance in nm	
Cations	Tetrahedral coordination	Octahedral coordination
Mn^{2+}	0.2041	—
Zn^{2+}	0.1981	—
Fe^{3+}	0.1858	0.2020
Mn^{3+}	—	0.2045
$\square$	0.2078	0.2245
Fe^{2+}	0.2012	0.2138

TABLE V

LATTICE PARAMETER VALUES OF THE SPINEL PHASE FOR DIFFERENT STAGES OF OXIDATION

Sample C	Initial sample	After partial oxidation in region II with □ on *B*-sites	After total oxidation without phase transf. with □ on B-sites	After total oxidation and formation of two cluster Ref. (*15*)		After partial oxidation (regions I + II) precipitation in region III		
				I	II	550°C	575°C	620°C
Experimental parameter (nm)	0.8475	0.8413	—	0.8383	0.8439	0.8421	0.8431	0.8437
Theoretical parameter (nm)	0.8465	0.8412	0.8394	0.8360	0.8434	0.8415	0.8427	0.8438

and the cationic distribution of the spinel phase containing the totality of zinc may be formulated as follows:

$$(Zn^{2+})_A(Fe^{3+}_{1.48}Mn^{3+}_{0.52})_B\,O_4^{2-}. \qquad (11)$$

The fact that the phase transformation occurs from a cation deficient spinel with the presence of unoxidized Mn^{2+} ions (Eq. 6) suggests that above 450°C the following reaction take place:

$$(Zn^{2+}_{0.429}Mn^{2+}_{0.152}Fe^{3+}_{0.419})_A\ (Fe^{3+}_{1.536}Mn^{3+}_{0.325}\,\square_{0.139})_B$$

$$O_4^{2-} + \frac{\delta}{4}O_2 \rightarrow \frac{8+\delta}{8}$$

$$\left[1 - \Delta\left(\frac{Zn^{2+}_{3.482}}{t}\,\frac{Mn^{2+}_{8(0.152-\delta)}}{t}\,\frac{Fe^{3+}_{1+8\delta-4.648}}{t}\right)_A\right.$$

$$\left.\left(\frac{Fe^{3+}_{4.288-8\delta}}{t}\,\frac{Mn^{3+}_{8(0.325+\delta)}}{t}\,\frac{\square_{3t-6.888}}{t}\right)_B\right]^{O_4^{2-}}$$

$$\cdots + \frac{8+\delta}{8}\left[\tfrac{3}{4}\Delta\left(Fe^{3+}_{1.7}Mn^{3+}_{0.3}\right)\right]O_3^{2-} \qquad (12)$$

In this formula $t = (1 - \Delta)(8 + \delta)$, where δ and Δ were the oxidation and precipitation content, respectively.

The valence change of manganese ions and cation vacancy elimination occur within the spinel phase when the rhombohedral phase is segregated. This is consistent with the evolution of lattice parameter in region III and with one constant cell parameter for the precipitated phase $\alpha - (Fe^{3+}_{1.7}Mn^{3+}_{0.3})_B\,O_3^{2-}$.

Conclusion

Our DTG measurements supported by X-ray analysis show that at heating temperatures in air below about 500°C, a cation deficient spinel represented by Eq. (6) is produced independently of preparation method. It is established that the percentage of oxidized manganese slightly depends on crystallite size and an approximately constant value 60% was found for all samples. In manganese substituted magnetites (13), the percentage of oxidized Mn^{2+} ions was also found to be about 60% for all concentrations of Mn. Because of the close resemblance between the lattice structure of this defect spinel and γ-Fe_2O_3 we expect that similar to γ-Fe_2O_3, the vacancies associated with the missing metal atoms are located in *B*-sites. After cation deficient spinels have been formed as intermediate phases, a phase transformation during heating above 500°C still occurs and means to the formation of a spinel phase containing the totality of zinc with progressive elimination of vacancies

by oxidation of remaining Mn^{2+} ions that competes with the presence of a rhombohedral phase.

References

1. P. J. Van der Zaag, M. T. Johnson, A. Noordermeer, P. T. Por, and M. Th. Rekveldt, *J. Magn. Magn. Mater.* **99,** L1 (1991).
2. P. Perriat and M. Abouaf, "Euro-Ceramics: Applied Sci." Vol. 3, p. 237, Elsevier, Amsterdam (1989).
3. P. Perriat, R. Lebourgeois, and J. L. Rolland, "6th International Conference on Ferrites," Tokyo, 1992, to be published.
4. B. Gillot, M. L. Guendouzi, P. Tailhades, and A. Rousset, *React. Solids* **1,** 189 (1986).
5. J. M. Hastings and L. M. Corliss, *Phys. Rev.* **104,** 328 (1956).
6. Sh. Bashkirov, A. B. Liberman, and V. I. Sinyavskii, *Fiz. Tverd. Tela.* **14,** 3264 (1972).
7. T. Kubo, A. Hirai, and H. Abe, *J. Phys. Soc. Jpn.* **26,** 1074 (1969).
8. T. Abbas, Y. Khan, M. Ahmed, and S. Anwar, *Solid State Commun.* **82,** 701 (1992).
9. M. El Guendouzi, K. Sbai, P. Perriat, and B. Gillot, *Mater. Chem. Phys.* **25,** 429 (1990).
10. C. Michalk, *J. Magn. Magn. Mater.* **68,** 157 (1987).
11. P. Tailhades, M. El Guendouzi, A. Rousset, and B. Gillot, *C.R. Acad. Sci. Paris Ser. II* **299,** 13 (1984).
12. K. Suresh, G. V. Mahesh and K. C. Patil, *J. Thermal Anal.* **35,** 1137 (1989).
13. M. Laarj, I. Pignone, M. El Guendouzi, P. Tailhades, A. Rousset, and B. Gillot, *Thermochim. Acta* **152,** 187 (1989).
14. I. R. Leith and M. G. Howder, *Appl. Catal.* **37,** 75 (1988).
15. C. Michalk, E. Richter, and Chr. Semmelhack, *Hermsdorfer Techn. Mitt.* **71,** 2253 (1987).
16. C. Michalk and W. Berr, Hermsdorfer Techn. Mitt., **71,** 2257 (1987).
17. P. Poix, "Liaison interatomique et propriétés physiques des composés minéraux," Seides, Paris, 82 (1968).
18. P. Tailhades, A. Rousset, R. Bendaoud, A. R. Fert, and B. Gillot, *Mater. Chem. Phys.* **17,** 521 (1987).